# Different Approaches to Multiedge Detection in SAR Images

*Roger Fjørtoft*[1,2] *Armand Lopès*[1] *Philippe Marthon*[2] *Eliane Cubero-Castan*[3]

[1]CESBIO (UMR 5639 CNES/CNRS/UPS), 18 avenue Edouard Belin, Bpi 2801, 31401 Toulouse cedex 4, France
Phone: (33) 5-61-55-85-39 Fax: (33) 5-61-55-85-00 E-mail: Roger.Fjortoft@cesbio.cnes.fr Armand.Lopes@cesbio.cnes.fr

[2]ENSEEIHT (LIMA-IRIT-URA CNRS 1399), 2 rue Camichel, Bp 7122, 31071 Toulouse cedex 7, France
Phone: (33) 5-61-58-83-53 Fax: (33) 5-61-58-83-53 E-mail: Philippe.Marthon@enseeiht.fr

[3]CNES – French Space Agency (DGA/SH/QTIS), 18 avenue Edouard Belin, 31401 Toulouse cedex 4, France
Phone: (33) 5-61-27-46-12 Fax: (33) 5-61-27-31-67 E-mail: Eliane.Cubero-Castan@cnes.fr

Abstract -- Edge detection is a fundamental issue in image analysis. The presence of speckle, which can be modelled as a strong multiplicative noise, complicates edge detection in Synthetic Aperture Radar (SAR) images. Several statistical edge detectors have been developed specifically for such images, based on the hypothesis that only one step edge is present in the analyzing window. We here concentrate on the spatial aspect of edge detection in SAR images. Depending on the scene type and the size of the analyzing window, the monoedge hypothesis is violated more or less frequently. We present and compare three approaches to edge detection in a multiedge context: an optimum non-adaptive operator, a spatially adaptive operator and multiscale analysis.

## INTRODUCTION

SAR images and images from other imaging systems relying on coherent illumination are characterized by strong intensity fluctuations known as speckle. In SAR imagery speckle is generally modelled as a multiplicative, Gamma-distributed random noise with unity mean and variance equal to the inverse of the Equivalent Number of Independent Looks (ENIL) [3].

Gradient-based edge detectors, developed for optical images, perform poorly when applied to SAR images. This is mainly due to the multiplicative nature of speckle. A basic experience is that gradient-based operators, which basically compute a difference of local mean values on opposite sides of the central pixel, detect more false edges in areas of high reflectivity than in areas of low reflectivity. To overcome this problem, several statistical edge detectors have been developed for SAR images based on the multiplicative noise model and the restrictive hypothesis that only one step edge is present in the analyzing window. Well-known examples of such monoedge detectors are the Ratio Of Averages (ROA) operator [1] and the Likelihood Ratio (LR) operator [2], which both yield a Constant False Alarm Rate (CFAR). The ROA operator coincides with the optimum LR operator when only the analyzing window is split in two equally sized halves.

The monoedge model is, however, not very realistic. To sufficiently suppress the influence of the speckle, relatively large analyzing windows must be used, and for most scene types several edges may then co-occur within a half-window. There are several ways of taking this situation into account.

## MULTIEDGE DETECTORS

The computationally most efficient approach is to use a non-adaptive operator designed for the multiedge case. We recently proposed a CFAR edge detector for SAR images which is optimum in the Minimum Mean Square Error (MMSE) sense for a stochastic multiedge model [4]. This operator computes a Ratio Of Exponentially Weighted Averages (ROEWA) on opposite sides of the central pixel in the horizontal and vertical directions. The slope of the exponential weighting function is controlled by a parameter $b$, which depends on the reflectivity mean and variance, the ENIL and the mean region width [4]. To make the operator independent of the scanning direction, we normalize each ratio to be superior to one by taking the maximum of the measured ratio and its inverse. The magnitude of the horizontal and vertical components yields an edge strength map, from which local maxima are extracted and attributed to edges.

The ROA operator is basically designed for the monoedge case, but by making the size and shape of the window scene adaptive it can face a multiedge situation. We have chosen an approach which is slightly different from the one proposed in [1]. We first fix the Probability of False Alarm (PFA), *ie* the probability of detecting an edge in a zone of constant reflectivity. The corresponding detection thresholds for all window sizes in the range of interest are calculated. We compute the ratio in the horizontal, vertical and diagonal directions, and take the maximum of each measured ratio and its inverse. To facilitate the comparison of results for windows of different sizes, each ratio is divided by the appropriate detection threshold. Normalized ratios superior to one thus indicate the presence of an edge. The overall maximum value, which is the strongest indication of an edge across the scales, is retained as the edge strength of the pixel. Local maxima of the edge strength map are considered as the most probable edge localizations.

Multiscale analysis consists in detecting characteristic scale-space signatures. When using the continuous wavelet transform, the Haar wavelet is optimum for edge detection in signals with multiplicative noise [6]. However, such wavelet-based detection schemes do not yield a CFAR, so we use a ratio rather than a difference of arithmetic averages on each scale. Each scale corresponds to a certain window size, and we suppose that the monoedge hypothesis is verified at least for some of the smaller windows. The identification of the characteristic signature by correlation is quite complicated for a two-dimensional signal, so we propose a far simpler detection method [5]. We first employ the ROA operator over a wide range of window sizes, normalizing by the detection threshold as in the adaptive case. Pixelwise averaging of the results on different scales gives the edge strength map.

The watershed algorithm [7] can be used to obtain closed, skeleton boundaries running through local maxima of the edge strength map. To suppress false edges due to speckle more efficiently, we introduce a threshold under which local maxima are ignored [8], or basin dynamics [9].

## COMPARISON

The test image we have used to compare the different approaches is composed of vertical lines of gradually increasing width from 1 to 10 and with contrast ratio 4. The ideal image

0-7803-3836-7/97/$10.00 © 1997 IEEE

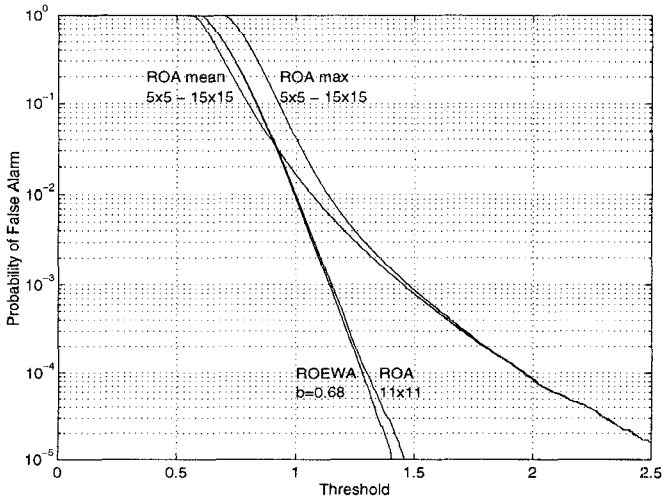


**Figure 1. PFA versus detection threshold.**

is multiplied by white noise with unity variance and mean to obtain a simulated 1-look image. As all edges are vertical, we compute ratios only in the horizontal direction. We take the ROA operator with window size 11 × 11 as a reference. The PFA was set to 1%, and the ratios were divided by the corresponding detection threshold as described above. We found the ROEWA operator with $b = 0.68$ to have the same speckle reduction capacity as the ROA operator with window size $11 \times 11$, and normalized the ratios of exponentially weighted averages by the same threshold. $b = 0.68$ corresponds to the theoretical optimum [5] for a mean region width of 5. The adaptive operator and the multiscale operator both used windows of size $5 \times 5$ through $15 \times 15$.

The experimental PFAs as a function of the threshold for all four methods are plotted in Fig. 1. We first note that threshold 1.0 as expected corresponds to a PFA of 1% for the fixed scale ROA operator. The PFA of the ROEWA operator coincides with that of ROA operator. Taking the mean ratio of arithmetic averages over several window sizes reduces the PFA for low thresholds, but for higher thresholds the PFA is higher than for the fixed scale operators. A threshold of 1.07 corresponds to a PFA of 1%. For the adaptive method, which takes the maximum ratio across the scales, the PFA graph lies above those of the other methods, but it converges towards that of the multiscale operator for high thresholds. According to Fig. 1, the threshold should be set to 1.13 for the adaptive operator to have the same PFA. Refer to [5] for information on the PFA in the multidirectional case.

A line of the ideal image is illustrated in Fig. 2. If we average a block of 11 speckled lines centered on a certain sample line, we obtain the intensities shown in Fig. 3. This illustrates the detection problem in the horizontal direction for the 11 × 11 ROA operator. Figs. 4 through 7 show the edge strengths obtained with the different operators centered on the sample line. The ideal edge positions are indicated by dotted vertical lines, and the threshold corresponding to a PFA of 1% is indicated by a horizontal dashed line in each case.

Let us now suppose that we retain local maxima over the threshold as edges, *cf* [8]. We see from Fig. 4 that the 11 × 11 ROA operator detects edges between lines of width 5 or higher. When the region width becomes smaller than the width of a half-window, the edge responses get much weaker, so that the edges are not detected with the PFA we have fixed. The ROEWA operator detects some edges at finer line widths, but some intermediate edges are lost and there is a spurious edge in pixel position 32. It should be noted that the test image is not a typical realization of the stochastic process corresponding to the multiedge model for which the ROEWA operator is optimum. When retaining the maximum ratio across the scales, we detect edges systematically down to line width 2, as can be seen from Fig. 6. For the operator which takes the mean ratio over different window sizes, we also detect edges down to line width 2, as shown in Fig. 7. As far as the edge localization precision is concerned, no significant differences can be observed between the two latter methods, but they both perform better than the ROEWA operator.

## CONCLUSION

In this article we compare three simple approaches to multiedge detection in SAR images. Tests on a simulated SAR image indicate that the two methods which rely on normalized ratios of arithmetic averages computed on different scales can detect edges that are closer together than the fixed-scale ROEWA operator with the same PFA. We have here only considered watershed thresholding of edge strength maps. To improve the edge detection, the expected evolution of an edge across the scales should be taken into account explicitly. The normalized ROA operator computed on different scales has a characteristic ridge as edge signature. A more advanced detection algorithm could follow this ridge from coarse scales and good noise reduction to finer scales and better edge localization.

## ACKNOWLEDGMENTS

This work is part of contract 833/CNES/96/0574/00. We thank the French Space Agency CNES for financial support.

## REFERENCES

[1] R. Touzi, A. Lopès, and P. Bousquet, "A statistical and geometrical edge detector for SAR images," *IEEE Trans. Geosci. Remote Sensing*, vol. 26, no. 6, pp. 764-773, November 1988.

[2] C. J. Oliver, D. Blacknell, and R. G. White, "Optimum edge detection in SAR," in *IEE Proc. Radar Sonar Navig.*, vol. 143, no. 1, February 1996.

[3] F. T. Ulaby, R. K. Moore, and A. K. Fung, *Microwave Remote Sensing*, vol. 3, Dedham, MA: Artech House, 1986.

[4] R. Fjørtoft, P. Marthon, A. Lopès, and E. Cubero-Castan, "Multiedge detection in SAR images," in *Proc. ICASSP*, vol. 4, Munich, Germany, April 1997, pp. 2761-2764.

[5] R. Fjørtoft, P. Marthon, and A. Lopès, "Multiresolution edge detection in SAR images," in *Proc. NORSIG*, Tromsø, Norway, May 1997.

[6] M. Chabert, J. Y. Tourneret, and Gilles Mesnager, "Edge detection in speckled SAR images using the continuous wavelet transform," in *Proc. IGARSS*, Lincoln, Nebraska, May 1996, pp. 1842-1844.

[7] L. Vincent and P. Soille, "Watersheds in digital spaces: An efficient algorithm based on immersion simulations", IEEE Trans. PAMI, vol. 13, no. 6, pp. 583-598, 1991.

[8] P. Marthon, B. Paci, and E. Cubero-Castan, "Finding the structure of a satellite image," in *Proc. EurOpto Image and Signal Processing for Remote Sensing*, vol. SPIE 2315, Rome, Italy, 1994, pp. 669-679.

[9] M. Grimaud, "A New Measure of Contrast: Dynamics," in *Proc. Image Algebra and Morphological Processing III*, vol. SPIE 1769, San Diego, July 1992, pp. 292-305.

Reprints of our communications can be downloaded from URL http://www.enseeiht.fr/Recherche/Info/Vision/Membres/RF/

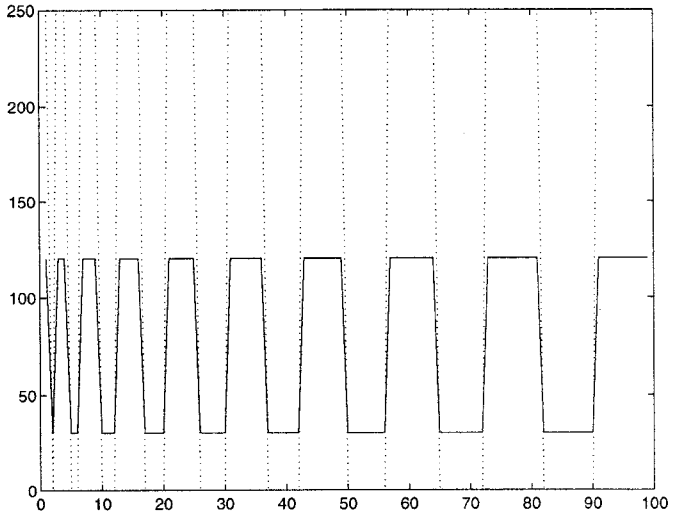


**Figure 2. Intensities of a sample line of the ideal test image.**

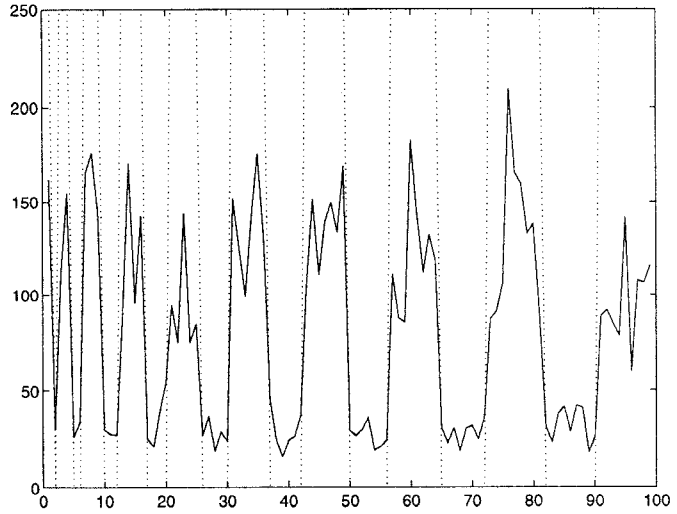


**Figure 3. Average intensities of a block of 11 lines of the speckled test image.**

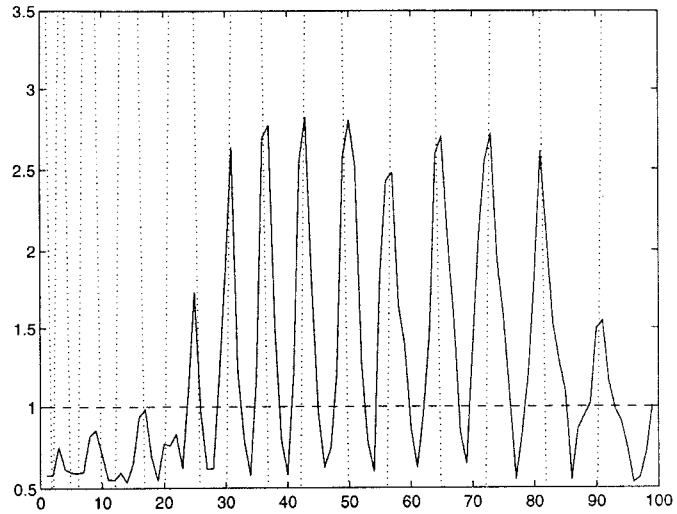


**Figure 4. Normalized ratios for a $11 \times 11$ window centered on the sample line.**

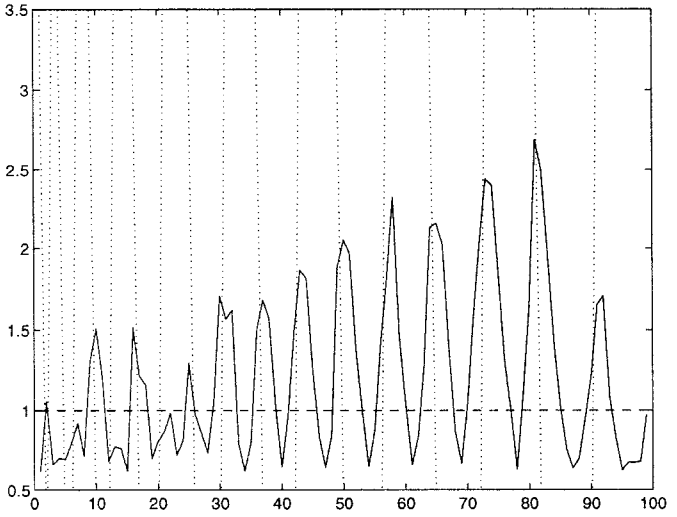


**Figure 5. Normalized ratios for the ROEWA operator with $b = 0.68$ centered on the sample line.**

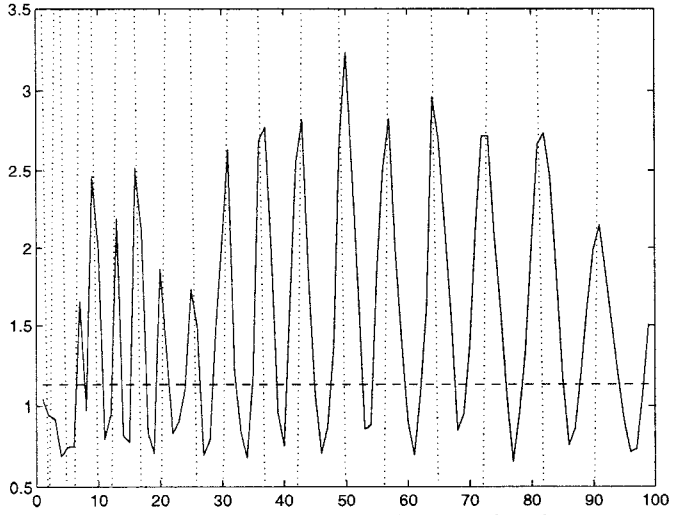


**Figure 6. Maximum of normalized ratios for $5 \times 5$ to $15 \times 15$ windows centered on the sample line.**

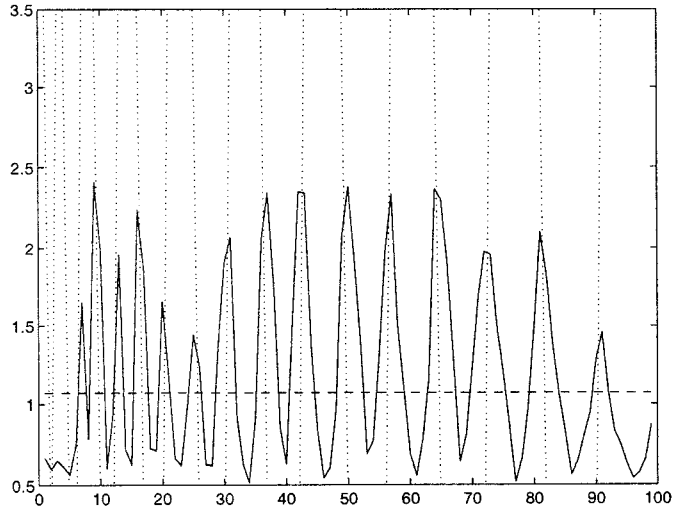


**Figure 7. Average of normalized ratios for $5 \times 5$ to $15 \times 15$ windows centered on the sample line.**